$GABA_A$ receptor membrane trafficking regulates spine maturity

Tija C. Jacob[a], Qin Wan[b], Mansi Vithlani[a], Richard S. Saliba[a], Francesca Succol[c], Menelas N. Pangalos[d], and Stephen J. Moss[a,e,1]

[a]Department of Neuroscience, Tufts University School of Medicine, Boston, MA 02030; [e]Department of Pharmacology, University College, London WC1E 6BT, United Kingdom; [c]Neuroscience and Brain Technology, The Italian Institute of Technology, 16163 Genova, Italy; [d]Neuroscience Discovery, Wyeth Research, Princeton, NJ 08852; and [b]National Institutes of Health, National Eye Institute, Bethesda, MD 20892

Edited by Richard L. Huganir, Johns Hopkins University School of Medicine, Baltimore, MD, and approved May 28, 2009 (received for review April 9, 2009)

$GABA_A$ receptors ($GABA_A$Rs), the principal sites of synaptic inhibition in the brain, are dynamic entities on the neuronal cell surface, but the role their membrane trafficking plays in shaping neuronal activity remains obscure. Here, we examined this by using mutant receptor β3 subunits (β3S408/9A), which have reduced binding to the clathrin adaptor protein-2, a critical regulator of $GABA_A$R endocytosis. Neurons expressing β3S408/9A subunits exhibited increases in the number and size of inhibitory synapses, together with enhanced inhibitory synaptic transmission due to reduced $GABA_A$R endocytosis. Furthermore, neurons expressing β3S408/9A subunits had deficits in the number of mature spines and reduced accumulation of postsynaptic density protein-95 at excitatory synapses. This deficit in spine maturity was reversed by pharmacological blockade of $GABA_A$Rs. Therefore, regulating the efficacy of synaptic inhibition by modulating $GABA_A$R membrane trafficking may play a critical role in regulating spine maturity with significant implications for synaptic plasticity together with behavior.

endocytosis | inhibition | phosphorylation

Fast neuronal inhibition in the brain is largely mediated by $GABA_A$Rs, which are Cl- selective pentameric ligand-gated ion channels assembled from 7 subunit classes with multiple members; α (1–6), β (1–3), γ (1–3), δ, ε, θ, and π. Consensus opinion suggests that the majority of synaptic receptor subtypes are assembled from α1–3, β, and γ2 subunits. The accumulation of $GABA_A$Rs on the neuronal membrane is a critical factor in determining synaptic inhibition and is largely dependent on rates of receptor exo- and endocytosis (1). After ER assembly, $GABA_A$Rs are inserted in the neuronal plasma membrane primarily at extrasynaptic sites and access the inhibitory postsynaptic specialization via lateral diffusion where they are stabilized via interaction with complements of the subsynaptic cytoskeleton (2, 3). Extrasynaptic receptor populations exhibit short cell surface half-lives and are rapidly removed from the plasma membrane via clathrin dependent-endocytosis (2, 4).

The endocytosis of $GABA_A$Rs is facilitated via the direct binding of the intracellular domains of receptor β1–3, γ1–2, and δ subunits to the μ2 adaptin of the AP2 complex (μ2-AP2) (5, 6). Subsequent analysis has revealed the presence of a conserved basic patch-binding motif for μ2-AP2 within all receptor β subunits (7), which contains the principal sites of phosphorylation within $GABA_A$Rs for cAMP-dependent protein kinase and protein kinase C, residues S408/9 respectively (1). In keeping with this, in vitro studies showed reduced binding of the GST- β3 intracellular domain (ICD) to μ2-AP2 with phosphorylation at S408/9 (7).

To determine the significance of regulated $GABA_A$R endocytosis in a neuronal context and the physiological consequence of altered $GABA_A$R cell surface levels, we expressed receptor β3 subunits in which S408/9 have been mutated to alanines in neurons. This mutation dramatically increased the synaptic accumulation of $GABA_A$Rs by reducing their endocytosis and also increased the efficacy of neuronal inhibition. Neurons expressing mutated β3 subunits exhibited a significant decrease in the number of mature spines and an increase in the number of thin, filopodia-like protrusions, a phenomenon that was reversed by pharmacological blockade of $GABA_A$Rs. Our results demonstrate a critical role for endocytosis in regulating the number of $GABA_A$Rs at inhibitory synapses together with the strength of neuronal inhibition. Moreover, they identify a role for GABAergic inhibition as a determinant of spine maturity, and thus a key mechanism for producing prolonged changes in neuronal activity.

Results

Mutation of S408/9 to Alanines Decreases the Binding of the $GABA_A$R β3 Subunit to μ2-AP2. In vitro studies have demonstrated the presence of a basic patch endocytosis motif conserved in all $GABA_A$R β subunits, residues 401–412 in the case of the β3 isoform (7), with S408/9 sites as the principal sites of phosphorylation for cAMP-dependent protein kinase (PKA) and protein kinase (1). To further determine the structural requirements for the interaction of $GABA_A$R β3 subunits with μ2-AP2 we used in vitro binding assays. We expressed GST fusion proteins encoding wild-type and mutant forms of the intracellular domain of the β3 subunit where the S408/9 residues were mutated to alanines and examined their ability to bind μ2-AP2 labeled with [^{35}S]methionine (^{35}S-μ2). This revealed that alanine mutation of S408/9 significantly reduced binding of ^{35}S-μ2 to 58 $\pm$ 6% compared to GSTβ3 (Fig. 1*A*). We also compared the effects of phosphorylating S408/9 in GSTβ3 on binding of ^{35}S-μ2. Exposure of GSTβ3 to purified PKA in the presence of ATP reduced ^{35}S-μ2 binding to 6 $\pm$ 2% consistent with previous studies (Fig. S1*A*) (7). Thus the phosphorylation of S408/9 or their mutation to alanines reduces binding of μ2-AP2 to the $GABA_A$R β3 subunit.

Mutation of S408/9 Slows Endocytosis of the β3 Subunit in HEK-293 Cells and Neurons. To assess the significance of decreasing the ability of $GABA_A$Rs to interact with μ2-AP2 for the construction of inhibitory synapses in addition to the efficacy of neuronal inhibition, we created β3 subunits modified at their N terminus with pHluorin reporters (pH-sensitive GFP) and the minimal binding site for α-bungarotoxin (BBS) (8). These additions allow the monitoring of cell surface receptor populations in live neurons using pHluorin fluorescence or receptor insertion and endocytosis with fluorescent bungarotoxin (Bgt) and do not modify the assembly or functional properties of $GABA_A$Rs (2, 3). Transient expression of $^{BBS}\beta$3 and $^{BBS}\beta3^{S408/9A}$ subunits in HEK-293 cells produced proteins with molecular masses of ≈90 kDa, with similar levels of

Author contributions: T.C.J., M.V., M.N.P., and S.J.M. designed research; T.C.J., Q.W., M.V., R.S.S., and F.S. performed research; T.C.J. contributed new reagents/analytic tools; T.C.J., Q.W., M.V., R.S.S., and F.S. analyzed data; and T.C.J. and S.J.M. wrote the paper.

The authors declare no conflict of interest.

This article is a PNAS Direct Submission.

[1]To whom correspondence should be addressed at: Department of Neuroscience, Tufts University School of Medicine, 136 Harrison Avenue, Boston, MA 02030. E-mail: stephen.moss@tufts.edu.

This article contains supporting information online at www.pnas.org/cgi/content/full/0903943106/DCSupplemental.

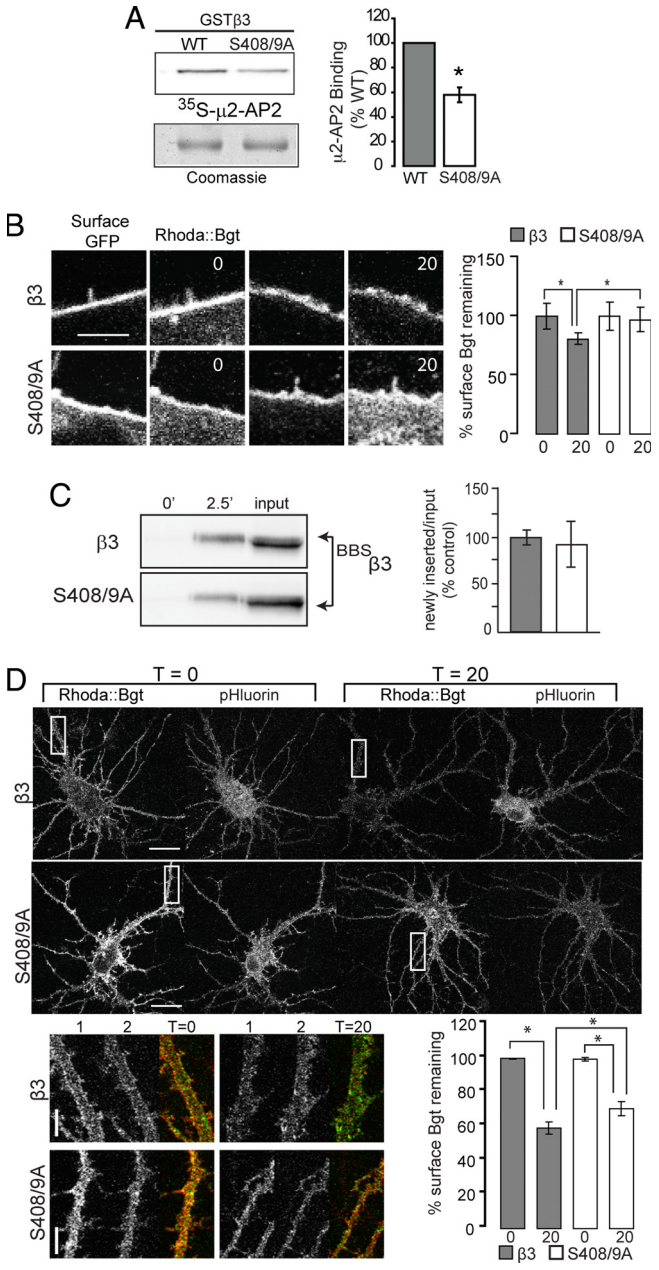

Fig. 1. Mutation of S408/9 decreases binding to μ2-AP2 and slows β3 subunit endocytosis. (*A*) Wild type (WT) and mutant GSTβ3 fusion proteins were separated by SDS-PAGE, transferred to nitrocellulose membrane and overlayed with in vitro translated (35)S m2-AP2. μ2-AP2 binding was visualized by autoradiography (*Top*), normalized to coomassie stain (*Bottom*), and expressed as a percentage of GST-β wild type control (*, $P < 0.001$, Student's *t* test, $n = 9$). *, significantly different to control. (*B*) HEK-293 cells endocytosis assay: surface $^{BBS}\beta$3 and $^{BBS}\beta3^{S408/9A}$ subunits were labeled with Rhoda::Bgt, washed, then incubated at 37°C with unlabeled Bgt for designated times before fixation and staining with anti-GFP antibody. Confocal images of individual cells at t0 and t20 min. Cell surface Rhoda::Bgt levels were quantified at t0 and t20 min for 10-μm lengths of plasma membrane. *, $P < 0.05$, *t* test, $n = 3$ transfections. (Scale bar, 5 μm.) (*C*) Insertion assay: nucleofected HEK-293 cells expressing $^{BBS}\beta$3 or $^{BBS}\beta3^{S408/9A}$ were incubated with unlabeled Bgt to block cell surface $^{BBS}\beta$3 at 12°C and then with biotinylated Bgt at 37°C for the times indicated. Cells were then lysed and Bgt-$^{BBS}\beta$3 complexes were precipitated with immobilized avidin and subjected to western blotting with mouse anti-GFP IgGs. Data represent means of newly inserted/input ratios normalized to $^{BBS}\beta$3. (*D*) Confocal images and quantification from hippocampal Bgt endocytosis assays. After a 10-min pretreatment with 150 μM tubocurare to block endogenous α7 nicotinic AChR receptors, hippocampal neurons expressing $^{BBS}\beta$3 or $^{BBS}\beta3^{S408/9A}$ subunits were labeled with 3 μg/mL Rhoda::Bgt and 150 μM tubocurare for 5 min, washed, then incubated at 37°C in media with 30 μg/mL unlabeled Bgt and 150 μM tubocurare for between 0–20 min. At t0 and t20 min, samples were removed and fixed. (Scale bars, 20 μm.) Magnified images of boxed dendritic regions are shown at t0 and t20 min (1, Rhoda::Bgt in red; 2, pHluorin fluorescence in green). (Scale bar, 5 μm.) Rhoda::Bgt levels on the cell surface at t0 and t20 were quantified for 2–3 dendritic regions per neuron and normalized to the construct expression level via pHluorin fluorescence for the same region. *, $P < 0.01$, 1-way ANOVA analysis and Tukey's multiple comparison tests, 18–20 neurons per construct, $n = 3$ cultures.

steady state accumulation and trafficking to the cell surface (Fig. S1*B* and *C*).

We next analyzed the ability of $^{BBS}\beta$3- or $^{BBS}\beta3^{S408/9A}$-containing $GABA_A$Rs to endocytose. HEK-293 cells expressing tagged β3 and S408/9A subunits were live-labeled with rhodamine conjugated Bgt (Rhoda::Bgt) for 5 min, washed extensively then incubated at 37°C in equilibrated media with 30 μg/mL unlabeled Bgt (to label any newly inserted receptors with a non fluorescent Bgt) for between 0–20 min, allowing measurement of Rhoda::Bgt loss due to receptor endocytosis. At 0 and 20 min time points, samples were removed, fixed, and stained with anti-GFP antibody under non-permeabilizing conditions to label the total surface receptor population. The fluorescence intensity of Rhoda::Bgt staining was measured at the periphery of expressing cells over time (Fig. 1*B*) and compared to the signal at 0 time, which was set to a value of 100%. $^{BBS}\beta3^{S408/9A}$ mutant receptors showed a decreased endocytic rate ($P < 0.05$), with 97.3 ± 10.3% surface Bgt signal remaining compared to the $^{BBS}\beta$3 control value of 80.8 ± 5.2% remaining at 20 min (Fig. 1*B*).

To control for possible differences in the insertion of $^{BBS}\beta$3 and $^{BBS}\beta3^{S408/9A}$ into the plasma membrane, expressing cells were labeled with unlabeled Bgt for 5 min at 12°C to block exo- and endocytosis, and then incubated in the presence of biotinylated Bgt for 2.5 min at 37°C. Bgt-labeled proteins were purified on avidin and immunoblotted with anti-β3 antibodies. After controlling for total expression levels it was evident that $^{BBS}\beta$3 and $^{BBS}\beta3^{S408/9A}$ exhibit similar levels of insertion (Fig. 1*C*). Significantly we have established that insertion of $GABA_A$Rs into the plasma membrane is linear at this time point (9, 10). Therefore mutation of S408/9 increases the cell surface stability of the β3 subunit in HEK-293 cells primarily by reducing its endocytosis.

Next we used Rhoda::Bgt to analyze the endocytosis of $GABA_A$Rs incorporating mutant β3S408/9A subunits in hippocampal neurons. Fourteen DIV neurons were transfected with $^{BBS}\beta$3 and $^{BBS}\beta3^{S408/9A}$ constructs and 48 h later, live neurons were labeled with Rhoda::Bgt, fixed and stained with anti-GFP antibody, and imaged by confocal microscopy. Quantification of expression levels from the pHluorin signal and cell surface levels with non-permeabilized anti-GFP staining respectively showed that $^{BBS}\beta$3 and $^{BBS}\beta3^{S408/9A}$ are expressed at equivalent total levels in neurons and access the cell surface with equal efficiency, where they assemble with other subunits to form heteromeric receptors (Fig. S1*D*). Bgt endocytosis assays in hippocampal neurons comparing average Rhoda::Bgt fluorescence intensity along a 20-μm dendritic length showed that $^{BBS}\beta3^{S408/9A}$ has a slight but significant ($P <$ 0.05) reduction in the rate of endocytosis (70.1 ± 4.1% remaining surface Bgt) when compared to control (58.7 ± 3.6% remaining surface Bgt) (Fig. 1*D*). Together these data suggest that mutation of S408/9 in neurons decreases the endocytic rate of heteromeric β3 subunit containing $GABA_A$Rs thereby increasing receptor cell surface stability.

Chronic Expression of $^{BBS}\beta$3 and $^{BBS}\beta3^{S408/9A}$ Mutant Subunits in Hippocampal Neurons. Next we assessed the long-term effects of decreased endocytosis of $GABA_A$Rs in neurons by nucleofecting hippocampal neurons with $^{BBS}\beta$3 and $^{BBS}\beta3^{S408/9A}$ mutant subunits on the day of plating. Live imaging revealed the tagged β3 subunit

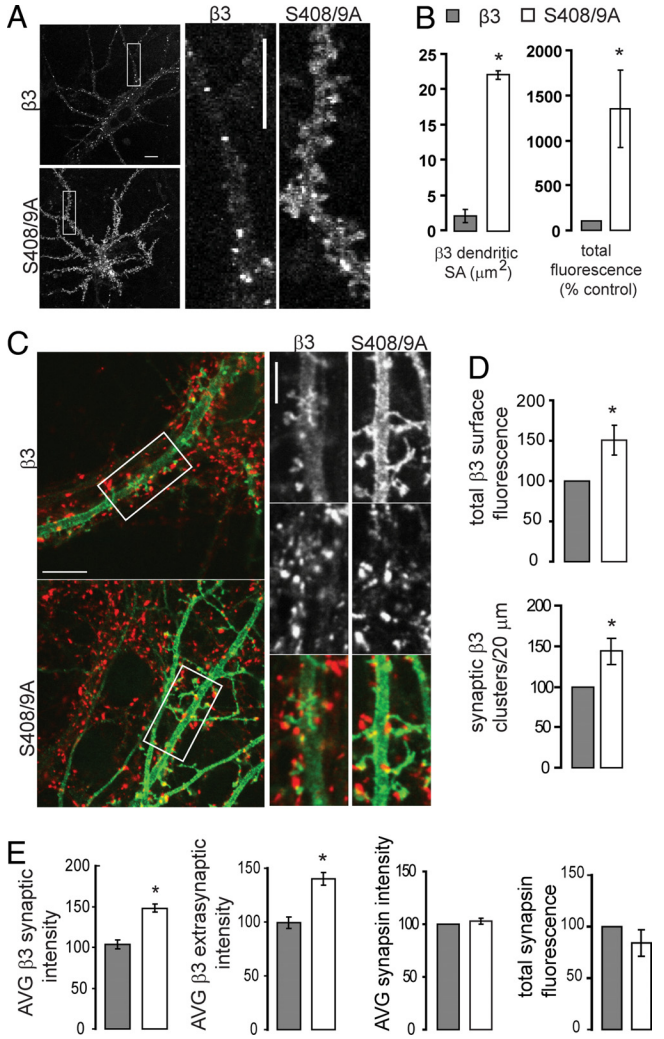

Fig. 2. Chronic expression of β3S408/9A increases the cell surface accumulation of $GABA_A$Rs containing β3 subunits. (*A*) Live confocal images of hippocampal neurons expressing pHluorin tagged β3 and β3S408/9A subunits maintained at 37°C in extracellular Hepes based buffer. The β3 subunit [as reported earlier (3)] and S408/9A mutant subunits assemble in diffuse and clustered receptor populations. (Scale bars, 10 μm.) (*B*) The area and total fluorescence level of the surface pHluorin signal of 20-μm long dendritic regions were quantified for β3 and β3S408/9A subunits. (*C–E*) Hippocampal neurons chronically expressing $^{BBS}\beta3$ or $^{BBS}\beta3^{S408/9A}$ subunits were fixed and stained under nonpermeant conditions with anti-GFP antibody (green), then permeabilized and stained with anti-synapsin antibody to mark presynaptic terminals (red). (Scale bar, 10 μm.) Also shown are enlargements of boxed areas. (Scale bar, 5 μm.) (*D*) Quantification of surface $^{BBS}\beta3$ or $^{BBS}\beta3^{S408/9A}$ total fluorescence by anti-GFP staining. The density of tagged β3 clusters colocalizing with synapsin per 20 μm of dendritic length was measured. (*E*) Quantification of average $^{BBS}\beta3$ or $^{BBS}\beta\ 3^{S408/9A}$ surface fluorescence intensity changes at synaptic and extrasynaptic locations. Quantification of synapsin average intensity and total fluorescence levels. For all images, *, $P < 0.05$, significantly different to control, *t* test, 1–2 processes per neuron, 18–24 neurons per construct, $n = 3$ cultures.

assembles into diffuse and clustered surface $GABA_A$R populations (2, 3), as did the S408/9A mutant (Fig. 2*A*). Intensity measurements of the pHluorin cell surface signal from live confocal imaging studies performed in extracellular Hepes based buffer at 14–17 DIV revealed dramatically increased $^{BBS}\beta3^{S408/9A}$ surface levels when compared to neurons expressing the control β3 subunit (Fig. 2*A*). Quantification of 20 μm long dendritic regions revealed a 10-fold increase in dendritic surface area coverage for $^{BBS}\beta3^{S408/9A}$ (22.1 ± 3.2 μm^2) compared to control β3 (2.1 ± 0.6 μm^2) with a total surface fluorescence count of 1,346.8 ± 429.9 when compared to the normalized control value of 100 ($P < 0.05$; Fig. 2*B*). These live imaging studies show that with longer term $^{BBS}\beta3^{S408/9A}$ expression in neurons, reduced endocytosis leads to a dramatic increase in surface levels of $^{BBS}\beta3^{S408/9A}$ subunit containing $GABA_A$Rs, compared to control $^{BBS}\beta3$ neurons.

Mutation of S408/9 Increases the Accumulation of β3 Subunit Containing $GABA_A$Rs at Both Extrasynaptic and Synaptic Sites in Hippocampal Neurons. To further characterize $GABA_A$R cell surface distributions in neurons chronically expressing control $^{BBS}\beta3$ and $^{BBS}\beta3^{S408/9A}$ mutant subunits, immunofluorescence studies were performed on fixed neurons. Cell surface populations of neurons were labeled with anti-GFP antibody and following permeabilization, presynaptic sites were labeled with anti-synapsin 1 (Fig. 2*C*). This enabled us to quantify synaptic and extrasynaptic distributions of $^{BBS}\beta3$ and $^{BBS}\beta3^{S408/9A}$ and assess possible changes in the presynaptic terminal. Quantification of surface GFP labeling of nonpermeabilized neurons confirmed the live imaging results, with $^{BBS}\beta3^{S408/9A}$ expressing neurons having a significant increase ($P < 0.05$) in the total surface fluorescence of β3 containing $GABA_A$Rs ($^{BBS}\beta3^{S408/9A}$ total surface fluorescence = 150.5 ± 18.6% of normalized control) and an increased density of synaptic β3-containing $GABA_A$Rs (143.9 ± 16.2% of normalized control) (Fig. 2*D*). Despite the dramatic increase in cell surface receptor population, no significant presynaptic changes were observed, with the average synapsin fluorescence intensity and presynapse size (reported as total fluorescence) being unchanged (Fig. 2*E*). Fluorescence intensity measurements of surface $^{BBS}\beta3^{S408/9A}$ at synaptic locations (where it colocalized with synapsin presynaptic staining) and at extrasynaptic locations increased ($P < 0.05$) in a uniform fashion (synaptic levels = 140.1 ± 5.7% of normalized control, extrasynaptic levels = 148.1 ± 5.4) (Fig. 2*E*). Together these live and fixed imaging studies show that mutation of S408/9 promotes accumulation of β3-containing $GABA_A$Rs on the cell surface and increases the density of synaptic β3 clusters.

Neurons Expressing $^{BBS}\beta3^{S408/9A}$ Subunits Exhibit Enhanced Levels of GABAergic-Mediated Inhibition. To assess whether the enhanced accumulation of $^{BBS}\beta3^{S408/9A}$ on the neuronal plasma membrane at synaptic sites altered the efficacy of neuronal inhibition we compared the properties of mIPSCs in neurons nucleofected with GFP, $^{BBS}\beta3$, and $^{BBS}\beta3^{S408/9A}$ (Fig. 3*A*). mIPSCs were isolated by the inclusion of TTX, DAP5, and CNQX to block voltage-gated sodium channels, and glutamate receptors, respectively (4, 11). Under these conditions, the remaining events were blocked by picrotoxin confirming that they arise via the activation of $GABA_A$Rs (Fig. S2*A*). Comparing Gaussian distributions of mIPSC amplitudes in neurons expressing GFP with those expressing $^{BBS}\beta3^{S408/9A}$ and $^{BBS}\beta3$ subunits revealed that in neurons expressing $^{BBS}\beta3^{S408/9A}$ there was a uniform increase in amplitude for all events (Fig. S2*B* and *C*). Consistent with this, mean mIPSC amplitude in $^{BBS}\beta3^{S408/9A}$ expressing neurons was 55.5 ± 6.5 pA a value significantly larger ($P < 0.05$) than seen in neurons expressing GFP (32.5 ± 3.3 pA) (Fig. 3*B*). However in neurons expressing $^{BBS}\beta3$ mean mIPSC amplitude was similar to that seen in GFP expressing cells (35.6 ± 4.2 pA). In addition we examined the effects of mutating S408/9 on mIPSC kinetics. mIPSC decay was best fitted via a single exponential which revealed that τ_{decay} was similar in neurons expressing GFP (25.7 ± 1.0 ms), $^{BBS}\beta3$ (24.9 ± 2.1 ms), and $^{BBS}\beta3^{S408/9A}$ (26.2 ± 1.6 ms) (Fig. S2*D*). In contrast there was a small but significant decrease ($P < 0.05$) in 10–90% rise time in neurons expressing $^{BBS}\beta3^{S408/9A}$ compared to GFP (2.8 ± 0.3 vs. 3.8 ± 0.2 ms, respectively) an effect not seen in those expressing $^{BBS}\beta3$ (3.6 ± 0.2 ms) (Fig. S2*E*). This modified rise time is consistent with studies in recombinant expression systems suggesting that phosphorylation of β subunits can modify $GABA_A$R kinetics (12–14). mIPSC frequency was also significantly increased ($P <$

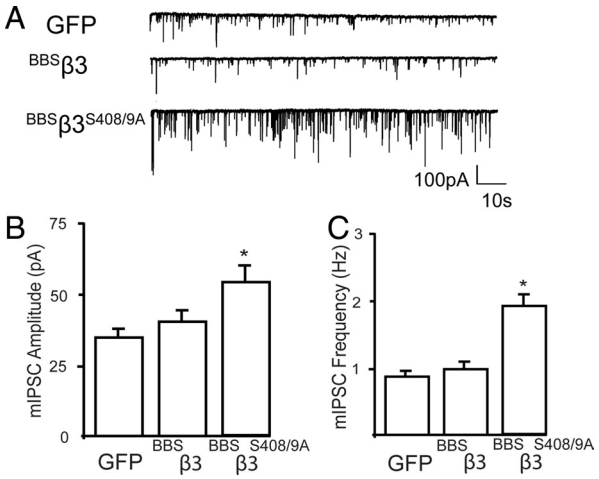

Fig. 3. Comparison of the properties of mIPSCs in hippocampal neurons expressing tagged $GABA_AR$ $\beta3$ subunits. (*A*) The properties of mIPSCs were compared in control (GFP) neurons and neurons expressing $^{BBS}\beta3$ or $^{BBS}\beta3^{S408/9A}$ subunits. (*B*) Bar graph of the mean mIPSC amplitudes from neurons transfected with GFP, $^{BBS}\beta3$, and $^{BBS}\beta3^{S408/9A}$. Data (mean ± SEM) are pooled from 7–12 cells for each condition. (*C*) mIPSCs frequencies were measured over a time course of 10 min for neurons expressing the respective constructs from each individual cell. *, $P < 0.05$, Kolmogorov–Smirnov test; $n = 8–10$ cells.

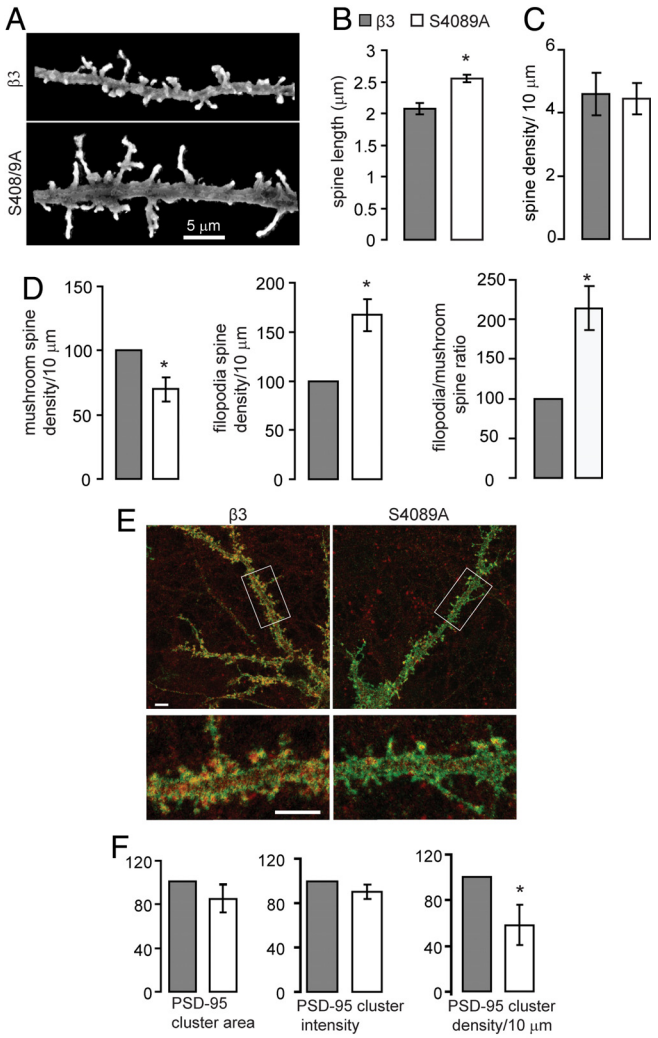

Fig. 4. Spine maturity is decreased in neurons expressing $\beta3$S408/9A subunits. (*A–F*) Hippocampal neurons chronically expressing $^{BBS}\beta3$ or $^{BBS}\beta3^{S408/9A}$ subunits were fixed and stained under permeabilized conditions with anti-GFP antibody. High magnification confocal z series through dendritic regions were acquired, and 3D reconstructions were used to analyze spine length, density, and morphology. (*A*) 3D reconstructions of confocal images from neurons expressing tagged $\beta3$ and $\beta3$S408/9A subunits.(*B*) Effects of $\beta3$S408/9A subunit on dendritic spine length (For *B–D*, *, $P < 0.05$, *t* test: number of spines measured = 525, 35–40 neurons per construct, $n = 3$ cultures). (*C*) Effects of $\beta3$S408/9A on dendritic spine density. (*D*) The number of mushroom and thin, filopodia-like spines per 10 μm was measured for both constructs. (*E*) Fifteen DIV $^{BBS}\beta3$ and $^{BBS}\beta3^{S408/9A}$ neurons were fixed and stained with anti-GFP antibody (green) to visualize dendritic processes and spines, followed by permeabilization and PSD-95 staining (red). Lower color panel is an enlargement of the boxed region above. (Scale bar, 5 μm.) (*F*) PSD-95 cluster area, intensity and density were quantified. For *E* and *F*, *, $P < 0.05$, *t* test: 20 neurons per construct from $n = 3$ cultures.

0.05) in neurons expressing $^{BBS}\beta3^{S408/9A}$ to 1.8 ± 0.4 Hz compared to those expressing GFP (0.91 ± 0.1 Hz), an effect not replicated in neurons expressing $^{BBS}\beta3$ (0.95 ± 0.2 Hz) (Fig. 3*C*). Presumably this increase is due to the recruitment of mIPSCs previously below the threshold of detection, owing to an increased number of postsynaptic $GABA_ARs$. This suggestion is supported by our observation that in neurons expressing ^{BBS} $\beta3^{S408/9A}$ the amplitude of all events is increased. $\beta3$ subunits can access the plasma membrane in expression systems as homomers where they form spontaneously open Cl^- permeable ion channels that are not activated by GABA or other receptor agonists, this behavior is suppressed by co-expression with receptor α and γ subunits (15, 16). Given that we specifically measure mIPSCs that by definition result from the spontaneous release of GABA these events will not contribute to our functional analysis. Thus consistent with our imaging studies neurons expressing $^{BBS}\beta3^{S408/9A}$ exhibit increased levels of neuronal inhibition that are likely to result from the increase in cell surface expression levels of heteromeric GABA-gated receptors.

Spine Maturity Is Decreased in Neurons Expressing $^{BBS}\beta3^{S408/9A}$ Subunits. Morphological characterization of neurons chronically expressing $^{BBS}\beta3$ and $^{BBS}\beta3^{S408/9A}$ was performed by confocal microscopy, using 3D reconstructions of Z series of permeabilized neurons stained with anti-GFP to fully visualize the dendrite and spine protrusions (Fig. 4*A*). Analysis of spine length and density revealed that S408/9A neurons had an increase in average spine length ($^{BBS}\beta3^{S408/9A}$ = 2.55 ± 0.09 μm, $^{BBS}\beta3$ = 2.08 ± 0.06 μm, $P < 0.05$) while spine density remained constant ($^{BBS}\beta3^{S408/9A}$ = 4.5 ± 0.5 spines/10 μm, $^{BBS}\beta3$ = 4.6 ± 0.7 spines/10 μm) (Fig. 4*B* and *C*). The cumulative distribution of all spine lengths was shifted to the right in $^{BBS}\beta3^{S408/9A}$ neurons when compared to control (Fig. S1*F*). Spine measurements were also performed with a fluorophore expressed independent of the tagged $\beta3$ $GABA_AR$ by conucleofecting a membrane-targeted GFP (Lck-GFP) with $^{BBS}\beta3$ and $^{BBS}\beta3^{S408/9A}$, producing similar results (Fig. S3*A* and *B*). Detailed assessment of spine morphology showed that in $^{BBS}\beta3^{S408/9A}$ neurons the density of mushroom-type spines had decreased ($^{BBS}\beta3^{S408/9A}$ = 69.7 ± 9.1% of control $^{BBS}\beta3$ density), while the filopodia-like spine density was increased ($^{BBS}\beta3^{S408/9A}$ = 167.2 ± 16.3% of control $^{BBS}\beta3$ density) ($P < 0.05$; Fig. 4*D*). This produced a shift in filopodia/mushroom-shaped spine ratio from 1:1 in control $^{BBS}\beta3$ neurons to 2:1 in $^{BBS}\beta3^{S408/9A}$ expressing neurons (Fig. 4*D*). The increased density of filopodia-like spines and the overall increase in spine lengths suggests that chronically $^{BBS}\beta3^{S408/9A}$ expressing neurons may have less mature dendritic spines. Acute transfection of $^{BBS}\beta3^{S408/9A}$ does not alter spine characteristics suggesting that enhanced cell surface $GABA_AR$ levels inhibit maturation on a developmental timescale (Fig. S1*E*).

PSD-95, a member of the membrane associated guanylate kinase family, is required for spine stabilization: PSD-95 overexpression results in increased spine head size maturity, and density (17), while

RNAi knockdown lead to immature spines with an increased rate in spine turnover (18). We used confocal microscopy to quantify PSD-95 expression in $^{BBS}\beta3^{S408/9A}$ expressing neurons, and observed a significant decrease ($P < 0.05$) in PSD-95 density to 58 ± 17% of $^{BBS}\beta3$ control levels (Fig. 4*E* and *F*). PSD-95 cluster area and intensity appeared to decrease, but these changes were not significant. Together with the electrophysiological measurements showing increased levels of inhibition in neurons expressing $^{BBS}\beta3^{S408/9A}$, these data suggest that decreased $GABA_AR$ endocytosis results in higher surface $GABA_AR$ levels and may inhibit spine maturation.

Pharmacological Blockade of $GABA_ARs$ Facilitates Spine Maturation in Neurons Expressing $^{BBS}\beta3^{S408/9A}$ Subunits. To determine if increased inhibition through higher $GABA_AR$ cell surface levels was responsible for the spine phenotype in $^{BBS}\beta3^{S408/9A}$ expressing neurons, we performed pharmacological blockade of $GABA_ARs$ with picrotoxin. Fourteen to 17 DIV neurons chronically expressing $^{BBS}\beta3$ and $^{BBS}\beta3^{S408/9A}$ were treated for 24 h with 50 μM picrotoxin or no drug, fixed, and stained with anti-GFP to visualize dendritic processes and spines (Fig. 5*A* and *B*). Picrotoxin treatment reversed the increased spine length in $^{BBS}\beta3^{S408/9A}$ neurons, reducing average spine length from 2.55 ± 0.09 μm to 1.98 ± 0.19 μm, equivalent to the spine length of control or picrotoxin treated $^{BBS}\beta3$ neurons, respectively ($^{BBS}\beta3$ control = 2.08 ± 0.06, ptx treated $^{BBS}\beta3$ = 2.00 ± 0.20 μm) (Fig. 5*C*). Twenty-four hours picrotoxin treatment also significantly increased ($P < 0.05$) the density of spines in $^{BBS}\beta3$ and $^{BBS}\beta3^{S408/9A}$ up to 66% (# spines per 10 μm for $^{BBS}\beta3$ control = 4.60 ± 0.67, ptx treated $^{BBS}\beta3$ = 7.06 ± 0.94, control $^{BBS}\beta3^{S408/9A}$ = 4.45 ± 0.49, ptx treated $^{BBS}\beta3^{S408/9A}$ = 6.65 ± 0.85). The ability of picrotoxin treatment to reverse the $^{BBS}\beta3^{S408/9A}$ spine defect suggests that higher $GABA_AR$ surface levels and increased inhibition are specifically responsible for the observed defect in spine maturation.

Discussion

Inhibitory synaptic transmission is reliant on the accumulation of $GABA_ARs$ at postsynaptic sites, a process that depends on their relative rates of exo- and endocytosis (1). Recruitment of $GABA_ARs$ into the endocytic pathway is facilitated via the interactions of the intracellular domains of receptor β1–3 and γ2 subunits with μ2-AP2 (7, 11). In vitro studies identified the presence of a basic patch μ2-AP2 binding motif between residues 401–412 for the β3 subunit (7) and showed that phosphorylation of S408/9 sites, the principal sites of phosphorylation for cAMP-dependent protein kinase (PKA) and protein kinase C (1), inhibits binding of μ2-AP2 to the β3 subunit. Whilst acute blockade of β3 subunit binding to μ2-AP2 can increase mIPSC amplitude, its significance for the construction of inhibitory synapses and in shaping neuronal activity remained to be elucidated (7).

We directly tested the role that S408/9 plays in mediating the binding of the β3 subunit to μ2-AP2. Mutation of S408/9 to alanines decreased the level of μ2-AP2 binding to the β3 subunit, an effect similar to that seen upon their phosphorylation. To test the consequences of reducing binding of μ2-AP2 to the β3 subunit for $GABA_AR$ membrane trafficking, we initially compared the exo- and endocytosis of homomeric β3 subunits modified with N-terminal pHluorin and BBS reporters when expressed in HEK-293 cells. Mutation of S408/9 had little effect on receptor exocytosis, but dramatically slowed their endocytosis as measured by fluorescent imaging with Bgt. In keeping with our experiments in HEK-293 cells, hippocampal neurons expressing $^{BBS}\beta3^{S408/9A}$ subunits exhibited reduced $GABA_AR$ endocytosis. To assess the long-term effects of decreased endocytosis for neuronal $GABA_ARs$, E18 dissociated hippocampal neurons were nucleofected with β3 expression constructs and cultured for 14–17 DIV. Imaging of nucleofected neurons revealed a significant increase in the cell surface accumulation of $GABA_ARs$ containing $^{BBS}\beta3^{S408/9A}$ compared to those incorporating $^{BBS}\beta3$ subunits. Notably, enhanced global cell surface accumulation of $^{BBS}\beta3^{S408/9A}$ subunits led to an increase in the density of synaptic $^{BBS}\beta3^{S408/9A}$ clusters. In agreement with the increased accumulation of $GABA_ARs$ at synaptic sites, mIPSC amplitude and frequency were dramatically increased in neurons expressing $^{BBS}\beta3^{S408/9A}$ compared to GFP but not in those transfected with $^{BBS}\beta3$. Thus consistent with our imaging studies, neurons expressing $^{BBS}\beta3^{S408/9A}$ subunits have increased levels of GABAergic inhibition. We also noted that the rise times of mIPSCs were decreased in neurons expressing $^{BBS}\beta3^{S408/9A}$ subunits. This may suggest that in addition to altering endocytosis, S408/9 mutation or their modification via phosphorylation may also modulate $GABA_AR$ kinetics (12–14).

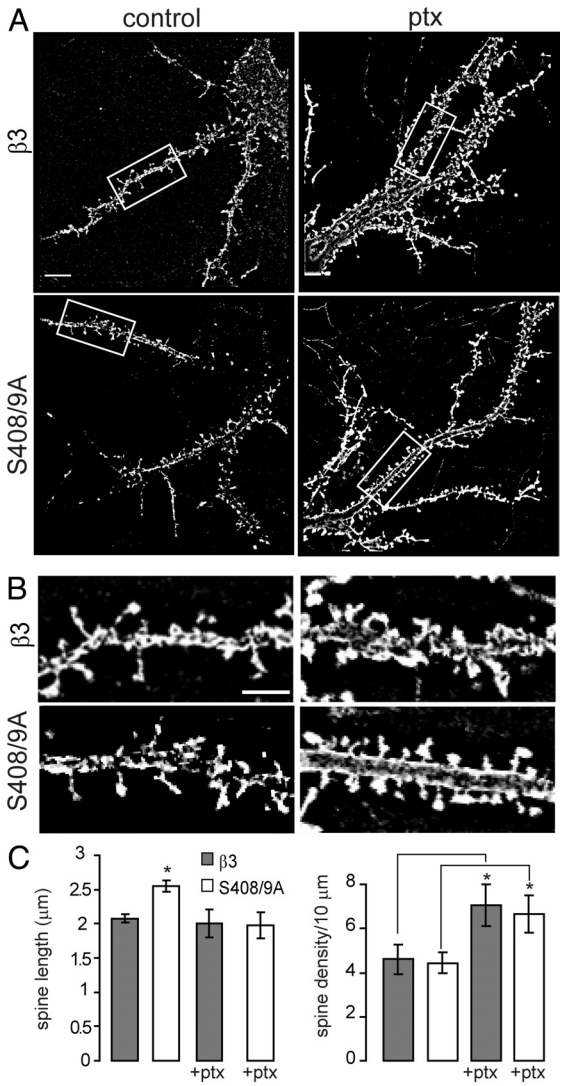

Fig. 5. Pharmacological blockade of $GABA_ARs$ enhances spine maturity in neurons expressing β3S408/9A subunits. (*A* and *B*) Fourteen to 17 DIV $^{BBS}\beta3$ and $^{BBS}\beta3^{S408/9A}$ neurons with and without a 24-h 50 μM picrotoxin (ptx) treatment were fixed and stained with anti-GFP antibody to visualize dendritic processes and spines. [Scale bar, 10 μm (*A*), 5 μm (*B*).] (*C*) Spine length and density were quantified (*, $P < 0.05$, *t* test: 20 neurons per construct, $n = 3$ cultures).

To begin evaluating the role that increased neuronal inhibition may play in regulating neuronal function, we used high resolution confocal imaging to compare the dendritic spine morphology of neurons expressing $^{BBS}\beta3$ and $^{BBS}\beta3^{S408/9A}$ subunits. The formation of new dendritic spines in the developing hippocampus is characterized by the formation of filopodia, some of which successfully

find a presynaptic terminal and then become spines with synapses, while others withdraw back to the dendrite to form shaft synapses (19). Thin or filopodia-like spines are considered to be less mature than mushroom spines which have larger, more complex post synaptic densities (PSDs) with a higher density of glutamate receptors and are far more likely to contain smooth endoplasmic reticulum (SER) and polyribosomes that promote local protein synthesis (19). Compared to control $^{BBS}\beta3$ neurons, $^{BBS}\beta3^{S408/9A}$ neurons showed an increase in average spine length and twice as many thin, filopodia-like spines as mushroom-type spines, although total spine density was unchanged. The increase in ratio of thin, filopodia-like spines to mushroom spines indicates that $^{BBS}\beta3^{S408/9A}$ expressing neurons may have less mature dendritic spines. Furthermore, $^{BBS}\beta3^{S408/9A}$ neurons showed a decrease in the density of PSD-95, consistent with the increased prevalence of immature filopodia-like spines. Picrotoxin treatment reversed the effect of increased spine length in $^{BBS}\beta3^{S408/9A}$ neurons, restoring spine lengths to control levels, suggesting that increased inhibition through higher $GABA_AR$ surface levels is specifically responsible for the observed defect in spine maturation.

As the primary site for excitatory synapses, alterations in dendritic spine morphology have mostly been considered from the perspective of increased or decreased excitatory activity. However, our data suggests that appropriate regulation of GABAergic inhibition through control of $GABA_AR$ cell surface levels may play as critical of a role in spine maturation. We have illustrated that reducing the association of $\mu2$-AP2 with the $\beta3$ subunit increases the accumulation of $GABA_ARs$ on the neuronal cell surface together with the efficacy of GABAergic inhibition, a phenomenon that reduces spine maturity. Therefore, modulating the endocytosis of $GABA_ARs$ may have long-term effects on neuronal excitation, synaptic plasticity, and behavior.

Materials and Methods

Cell Culture. HEK-293 cells were transfected as previously described (9). Hippocampal cultures were prepared from embryonic day 18 (E18) rats and constructs were nucleofected at plating (Amaxa) for chronic expression (3). Neurons were transiently transfected with Lipofectamine (Invitrogen).

Antibodies and Expression Constructs. The $^{BBS}\beta3$ and GST-$\beta3$ construct have been described previously (2, 7). GST-$\beta3$S4089A and $^{BBS}\beta3^{S408/9A}$ were generated by standard molecular biology cloning techniques and sequenced fully. Anti-$\beta3$, anti-GFP, and anti-synapsin antibodies were used as previously reported (9). The membrane-targed GFP (Lck-GFP) has been described previously (20).

Overlay Assay. Proteins were separated by SDS/PAGE, transferred to nitrocellulose membrane and overlayed with in vitro translated (35)S-AP2-$\mu2$ adaptin (TNT quick transcription/translation kit, Promega). Bound material was visualized by autoradiography and normalized to coomassie stain.

Live Imaging. Measurements were made on 14–17 days in vitro (DIV) hippocampal neurons maintained at 37°C in a closed heated chamber continuously perfused with extracellular Hepes-buffered saline (containing in mM: 135 NaCl, 4.7 KCl, 10 Hepes, 11 glucose, 1.2 $MgCl_2$, and 2.5 $CaCl_2$, pH 7.4) and images were collected using a 60× oil immersion objective lens acquired using an Olympus confocal microscope. Data were analyzed blind to experimental condition with a Metamorph imaging system (Universal Imaging).

Electrophysiology. Miniature inhibitory postsynaptic currents (mIPSCs) were recorded from 14–21 DIV cultured hippocampal neurons in the whole-cell voltage-clamp configuration (−70 mV) as reported previously and outlined in detail in *SI Materials and Methods* (7, 9).

Membrane Insertion Assay. To measure insertion of $GABA_ARs$, expressing HEK-293 cells were exposed to 10 μg/mL unlabeled α-Bungarotoxin (Bgt) for 20 min at 12°C and incubated with 10 μg/mL biotin-conjugated Bgt at 37°C for 2.5 min to label newly inserted receptors. Following lysis, biotin-Bgt/$^{BBS}\beta3$ and biotin-Bgt/$^{BBS}\beta3^{S408/9A}$ complexes were purified on neutravidin and immunoblotted with anti-$\beta3$ antibodies (9).

$GABA_AR$ Endocytosis Assay. Fluorescent Bgt labeling and $GABA_AR$ endocytosis assays in HEK-293 cells and 14–16 DIV hippocampal neurons expressing $^{BBS}\beta3$ and $^{BBS}\beta3^{S408/9A}$ mutant subunits were performed using procedures described in the results and (2) with additional detail given in *SI Materials and Methods*.

Image Acquisition and Analysis of Fixed HEK-293 Cells and Neurons. Surface anti-GFP staining of $^{BBS}\beta3$ and $^{BBS}\beta3^{S408/9A}$ and synaptic quantification was done as described previously (9) and outlined in detail in *SI Materials and Methods*. Spine morphological characterization (length, density, and spine type) of control $^{BBS}\beta3$ and $^{BBS}\beta3^{S408/9A}$ mutant neurons was performed on 3D reconstructions of confocal z series acquired using a 3× zoom. Spine lengths were measured manually with Metamorph software by tracing from the spine head down to where the spine joined the dendritic surface. Spines were counted as mushroom-type if the spine head was wider than the spine neck, and filopodia-type if the spine head width was equal to the spine neck width. For the picrotoxin studies, 50 μM picrotoxin was added to the media for 24 h, then neurons were fixed, immunostained with anti-GFP, and confocal images were acquired. Monoclonal anti-PSD-95(Affinity Bioreagents, 1:1,000) was used to quantify PSD-95 cluster area, intensity, and density. All Metamorph analysis was done blind to experimental condition.

ACKNOWLEDGMENTS. We thank Margie Maronski from the Dichter laboratory for preparation of cultured hippocampal neurons. S.J.M. is supported by National Institute of Neurological Disorders and Stroke Grants 046478, 048045, 051195, 056359, and P01NS054900; the Medical Research Council U.K.; and the Wellcome Trust. R.S.S. is supported by a fellowship from the American Society for Epilepsy.

1. Jacob TC, Moss SJ, Jurd R (2008) GABA(A) receptor trafficking and its role in the dynamic modulation of neuronal inhibition. *Nat Rev Neurosci* 9:331–343.
2. Bogdanov Y, *et al.* (2006) Synaptic GABAA receptors are directly recruited from their extrasynaptic counterparts. *EMBO J* 25:4381–4389.
3. Jacob TC, *et al.* (2005) Gephyrin regulates the cell surface dynamics of synaptic GABAA receptors. *J Neurosci* 25:10469–10478.
4. Kittler JT, *et al.* (2000) Constitutive endocytosis of GABAA receptors by an association with the adaptin AP2 complex modulates inhibitory synaptic currents in hippocampal neurons. *J Neurosci* 20:7972–7977.
5. Haucke V, Wenk MR, Chapman ER, Farsad K, De Camilli P (2000) Dual interaction of synaptotagmin with mu2- and alpha-adaptin facilitates clathrin-coated pit nucleation. *EMBO J* 19:6011–6019.
6. Haucke V (2006) Cargo takes control of endocytosis. *Cell* 127:35–37.
7. Kittler JT, *et al.* (2005) Phospho-dependent binding of the clathrin AP2 adaptor complex to GABAA receptors regulates the efficacy of inhibitory synaptic transmission. *Proc Natl Acad Sci USA* 102:14871–14876.
8. Sekine-Aizawa Y, Huganir RL (2004) Imaging of receptor trafficking by using alpha-bungarotoxin-binding-site-tagged receptors. *Proc Natl Acad Sci USA* 101:17114–17119.
9. Saliba RS, Michels G, Jacob TC, Pangalos MN, Moss SJ (2007) Activity-dependent ubiquitination of GABAA receptors regulates their accumulation at synaptic sites. 27:13341–13351.
10. Saliba RS, Pangalos M, Moss SJ (2008) The ubiquitin-like protein Plic-1 enhances the membrane insertion of GABAA receptors by increasing their stability within the endoplasmic reticulum. *J Biol Chem* 283:18538–18544.
11. Kittler JT, et al. (2008) Regulation of synaptic inhibition by phospho-dependent binding of the AP2 complex to a YECL motif in the GABAA receptor {gamma}2 subunit. 105:3616–3621.
12. Hinkle DJ, Macdonald RL (2003) Beta subunit phosphorylation selectively increases fast desensitization and prolongs deactivation of alpha1beta1gamma2L and alpha1beta3gamma2L GABA(A) receptor currents. *J Neurosci* 23:11698–11710.
13. Porter NM, Twyman RE, Uhler MD, Macdonald RL (1990) Cyclic AMP-dependent protein kinase decreases GABAA receptor current in mouse spinal neurons. *Neuron* 5:789–796.
14. Brandon NJ, Jovanovic JN, Smart TG, Moss SJ (2002) Receptor for activated C kinase-1 facilitates protein kinase C-dependent phosphorylation and functional modulation of GABA(A) receptors with the activation of G-protein-coupled receptors. *J Neurosci* 22:6353–6361.
15. Wooltorton JR, Moss SJ, Smart TG (1997) Pharmacological and physiological characterization of murine homomeric beta3 GABA(A) receptors. *Eur J Neurosci* 9:2225–2235.
16. Taylor PM, et al. (1999) Identification of amino acid residues within GABA(A) receptor beta subunits that mediate both homomeric and heteromeric receptor expression. *J Neurosci* 19:6360–6371.
17. El-Husseini AE, Schnell E, Chetkovich DM, Nicoll RA, Bredt DS (2000) PSD-95 involvement in maturation of excitatory synapses. *Science* 290:1364–1368.
18. Ehrlich I, Klein M, Rumpel S, Malinow R (2007) PSD-95 is required for activity-driven synapse stabilization. *Proc Natl Acad Sci USA* 104:4176–4181.
19. Bourne JN, Harris KM (2008) Balancing structure and function at hippocampal dendritic spines. 31:47–67.
20. Benediktsson AM, Schachtele SJ, Green SH, Dailey ME (2005) Ballistic labeling and dynamic imaging of astrocytes in organotypic hippocampal slice cultures. *J Neurosci Methods* 141:41–53.